Geochemistry Geophysics Geosystems G3

Article
Volume 12, Number 4
1 April 2011
Q04009, doi:10.1029/2010GC003382
ISSN: 1525-2027

Published by AGU and the Geochemical Society

Anisotropic viscosity changes subduction zone thermal structure

Einat Lev

Department of Earth, Atmospheric and Planetary Sciences, Massachusetts Institute of Technology, 77 Massachusetts Avenue, Cambridge, Massachusetts 02139, USA

Now at Lamont-Doherty Earth Observatory, Columbia University, 61 Route 9W, Palisades, New York 10964, USA (einatlev@ldeo.columbia.edu)

Bradford H. Hager

Department of Earth, Atmospheric and Planetary Sciences, Massachusetts Institute of Technology, 77 Massachusetts Avenue, Cambridge, Massachusetts 02139, USA

[1] Abundant observations of seismic anisotropy in subduction zones attest that the material in the mantle wedge has a strong fabric and therefore should be mechanically anisotropic. In this paper, we examine the effect of anisotropic viscosity on the thermal structure of subduction zone mantle wedges and quantify its importance relative to other thermal and rheological factors. Using two-dimensional finite element kinematic models we find that anisotropic viscosity results in two substantial changes: a hotter slab-wedge interface and time variability of the melt production rate and excess temperatures. Although not as significant as the effect of temperature-dependent viscosity, anisotropy leads to an increase of up to 35°C in the temperature along the slab-wedge interface. A hotter slab-wedge interface can change the depth extent of the seismogenic zone, limit the depth to which hydrous minerals can carry water, and influence flux melting. Time variability of the thermal field is a novel result of adding anisotropic viscosity to our models. This time variability results from heterogeneity in material alignment and could explain temporal changes in subduction zone magmatism without invoking a change in the wedge geometry, slab age, or composition.

Components: 5500 words, 7 figures.

Keywords: subduction zones; anisotropy; mantle rheology; numerical modeling.

Index Terms: 8162 Tectonophysics: Rheology: mantle (8033); 8170 Tectonophysics: Subduction zone processes (1031, 3060, 3613, 8413).

Received 30 September 2010; **Revised** 22 February 2011; **Accepted** 27 February 2011; **Published** 26 April 2011.

Lev, E., and B. H. Hager (2011), Anisotropic viscosity changes subduction zone thermal structure, *Geochem. Geophys. Geosyst.*, *12*, Q04009, doi:10.1029/2010GC003382.

1. Introduction

[2] Subduction zones, where one tectonic plate plunges beneath its neighbor, are an important feature of plate tectonics. Subduction zones are often characterized by frequent and forceful seismic activity, as well as ample volcanism, and provide the major source of buoyancy driving plate motion. A key element in building an understanding of the subduction process is the development of physically consistent and accurate models, which include the necessary physical processes that affect the dynamics of subduction zones.

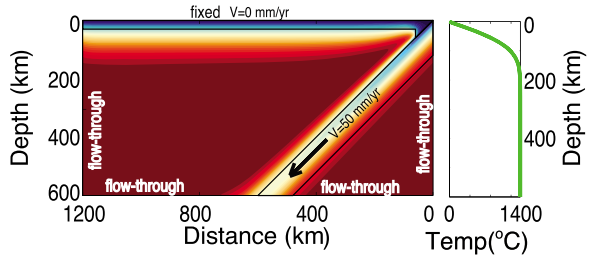

Figure 1. Model geometry and boundary conditions. (left) The temperature distribution after the model reaches a kinematic steady state. (right) The temperature profile used as a boundary condition along the side walls. This is the profile throughout the box width at time = 0.

[3] The thermal structure of the mantle wedge controls the distribution of melting, dehydration reactions, and seismicity in subduction zones. Physical parameters such as slab geometry, velocity, and mantle rheology influence the thermal structure of wedges; we focus here on the effects of anisotropic viscosity. Extensive modeling work has previously shown how the assumed rheology of subduction zone materials changes observables such as dynamic topography [e.g., *Gurnis*, 1993; *Billen et al.*, 2003], seismic anisotropy [*Long et al.*, 2007; *Kneller et al.*, 2008], volcanism and melting [*Kelemen et al.*, 2003], slab stagnation [*Torii and Yoshioka*, 2007], postseismic deformation [*Katagi et al.*, 2008], deep earthquakes [*Karato et al.*, 2001] and general dynamic behavior [e.g., *Kemp*, 1992; *Stein et al.*, 2004]. We demonstrate here that anisotropic viscosity, a factor almost certainly relevant to the mantle, changes the flow in the mantle wedge and alters its thermal structure.

[4] The strong seismic anisotropy that is a hallmark of subduction zones is commonly attributed to the alignment of anisotropic minerals by flow in the mantle wedge or below the subducting slab [*Savage*, 1999; *Hall et al.*, 2000]. An alternative source of seismic anisotropy is the alignment of melt inclusions or fluid-filled lenses [*Holtzman et al.*, 2003]. The global pattern of seismic anisotropy in subduction zones is complex: orientations vary from trench parallel to trench perpendicular and delay times of split shear waves range from barely measurable to a few seconds [e.g., *Long and Silver*, 2008].

[5] Many minerals have inherent plastic anisotropy, a result of differences among the strength of the various slip systems available for accommodating deformation at the crystal level. Olivine, the main constituent of Earth's upper mantle, is an example. Olivine deforms at least 10 times faster at a given stress when its easy slip system (slip in the *a* direction in the *b* plane, or (010) [100]) is aligned with the direction of shear stress compared to less favorable orientations, which requires activation of harder slip systems [e.g., *Durham and Goetze*, 1977; *Drury et al.*, 1991]. Alignment of weak phases such as melt can result in over an order of magnitude difference between the effective viscosities with respect to shearing parallel and orthogonal to the layers [e.g., *Treagus*, 2003].

[6] The abundance of observations of seismic anisotropy in subduction zones clearly indicates strong preferred orientation of minerals and heterogeneities on various length scales, and raises the question: If the strong preferred orientation of wedge materials has a mechanical expression, how will the resulting anisotropic viscosity influence the dynamics of subduction? This paper aims at answering this question with respect to the flow and resulting thermal structure of the mantle wedge.

[7] The influence of anisotropic viscosity on geodynamical flows has been demonstrated previously for thermal instabilities [*Richter and Daly*, 1978], thermal convection [*Saito and Abe*, 1984; *Honda*, 1986; *Christensen*, 1987], postglacial rebound [*Christensen*, 1987; *Wahr and Han*, 1997], oceanic plate dynamics [*Hearn et al.*, 1997] and lithospheric instabilities [*Lev and Hager*, 2008a]. Here we address the case of subduction. We describe results from a set of numerical experiments where subduction is driven kinematically. We find that anisotropic viscosity in the mantle wedge changes its thermal structure, leading to hotter temperatures at the slab-wedge interface and to time variability in the melting behavior.

2. Modeling Methodology

[8] In order to isolate the effects of anisotropic viscosity in a controlled way, our subduction models are kinematic: flow is driven only by the velocity we prescribe to the slab. This boundary condition drives flow in the wedge between the slab and the stagnant overriding plate. Thermal buoyancy is thus not included in our calculations. Figure 1 shows the model geometry and boundary conditions. We constructed a suite of models: a control model with isotropic mantle wedge material (IM hereafter) and models with anisotropic viscosity (AM* hereafter) spanning a range of magnitudes of anisotropy. We calculate the flow and the temperature fields in the

wedge in both configurations and compare the results. Our model design is similar to that used for the kinematic subduction community benchmark [*van Keken et al.*, 2008] and those used by *van Keken et al.* [2002] and *Kelemen et al.* [2003]. We confirmed the correctness of our code by running a simulation identical to the benchmark simulation and receiving the same result. We compare the slab-wedge temperatures in models of [*van Keken et al.*, 2008] with the results from an *Underworld* model that used the same geometry in Figure S1.[1]

2.1. Model Setup and Solution

[9] We solve the equations of conservation of mass, momentum and energy using the finite element code *Underworld* [*Moresi et al.*, 2007], which includes a formulation for anisotropic viscosity. We use a transversely isotropic symmetry for the viscosity, corresponding to a rheology with one dominant easy glide plane. While this symmetry is not fully equivalent to the symmetry of orthorhombic mantle constituent minerals such as olivine, in 2-D this suffices if using the most common kind of olivine fabric, the A type fabric. Transverse anisotropic viscosity can be described by two independent viscosities, a normal viscosity η_N and a shear viscosity η_S. The important parameter is the ratio between these two viscosities, which is commonly defined as $\delta = \frac{\eta_S}{\eta_N}$ [*Honda*, 1986]. In our most anisotropic model, we set δ to 0.1, in agreement with estimates for rocks and mantle minerals [*Durham and Goetze*, 1977; *Castelnau et al.*, 2008]. This model is called AM01, for "Anisotropic Model with δ = 0.1". Since the magnitude of the anisotropy of viscosity for mantle materials is not well constrained, we also ran models with viscosity ratio values of δ = 0.3, 0.5 and 0.7. We will refer to these models as AM03, AM05, and AM07, respectively. To verify that any changes we observed are due to the anisotropy and not to the overall reduction in effective viscosity of the wedge material, we ran a model with a viscosity just 30% of the original isotropic viscosity. Because buoyancy is not included, the absolute magnitude of the viscosity is not important, and, as expected, the results of the two isotropic models were identical to within numerical noise.

[10] The fabric we use for the anisotropic viscosity calculations is coupled to the flow. We track a set of over 1 million directors (oriented particles) distributed evenly throughout the mantle wedge. The directors represent normals to the plane of easy shear, and are rotated and stretched by the flow. The initial orientation of the easy glide planes is set to be random. New particles entering the model domain through the in-flow boundaries have random orientations. The orientation of the directors evolves according to the method described by *Mühlhaus et al.* [2002] and *Lev and Hager* [2008b].

[11] We use a non-Newtonian viscosity with a stress exponent n = 3.4 [*Hirth*, 2002]. While in early experiments we found, in agreement with *Long et al.* [2007], that the effect of including non-Newtonian viscosity on the flows was small, we include it for consistency: LPO development requires deformation in the dislocation creep regime, which implies a power law rheology. In all the models, viscosity follows an Arrhenius type rule, that is temperature dependent and pressure independent, shown to be crucial for melt production in similar kinematic models [*Kelemen et al.*, 2003]. The activation energy is 500 KJ mol^{-1}, within the range of values reported by *Hirth and Kohlstedt* [1995]. Heat sources associated with viscous dissipation and adiabatic decompression are not included in the energy calculation.

[12] Our model domain is a 1200 by 600 km 2-D box, discretized as a 256 by 128 regular finite element grid (Figure 1). The slab dips at 45° and moves at a constant velocity of 50 mm/yr. The top 30 kilometers of the overriding plate are fixed (V = 0). To avoid singularity, we followed the technique used by *van Keken et al.* [2008] and added a 30 km wide rigid "nose" at the wedge tip and a short ramp (18 km) of a linear increase in velocity immediately below the rigid nose. Thus the decoupling zone between the slab and the overriding plate, expressed as a discontinuity in velocity, reaches a depth of 60 km, close to the preferred distance of *Wada and Wang* [2009].

[13] The initial thermal profile in our models is an error function solution. The surface is kept at 0°C and the interior at 1400°C (=T_p, potential temperature). The initial thickness of the thermal boundary layer represents that of a 100 Myr old plate. The sides of the box keep the error function profile as boundary conditions. Thus, slab material entering the box through the right-hand side also has the same error function thermal profile. Slabs of lithospheric age of approximately 100 Myr are currently subducting in Tonga, Mariana, Western Aleutians, Kuril and the Caribbeans [*Molnar and Atwater*, 1978]. We run the models for 90 Myr,

[1] Auxiliary materials are available in the HTML. doi:10.1029/2010GC003382.

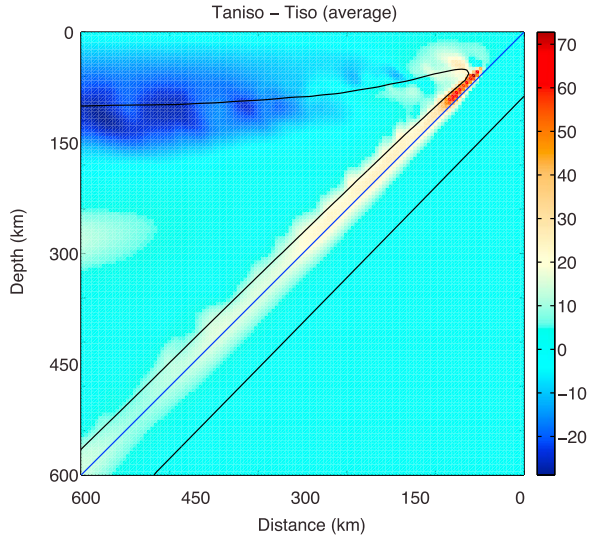

Figure 2. Time-averaged (over 30 Myr) difference in the temperature field between the anisotropic model AM01 and the isotropic model IM. Both models shown have temperature-dependent viscosity. Model AM01 is characterized by a thin warmer layer at the top of the slab and a cooler (by approx. 20°C) overriding lithosphere. The wedge corner shows the largest temperature difference: 65° hotter in AM01.

well beyond the time to reach a kinematic steady state in which the model velocities stabilize. We did not run the models to a full thermal steady state as this leads to thickening of the overriding conductive lid and prevents dry melting in the wedge.

3. Results

3.1. Differences in Thermal Structure

[14] We compare the thermal structure of a wedge with isotropic viscosity to that of a wedge with anisotropic viscosity by plotting the difference in temperature throughout the wedge for model AM01 (δ = 0.1) in Figure 2. A clear difference between the fields is the warmer slab-wedge interface and fore-arc region. Plotting the temperature along the slab-wedge interface (Figure 3), we see that in all cases, the anisotropy leads to a warmer slab-wedge interface, by up to 60 degrees. The heating is directly proportional to the strength of the anisotropy, with the more weakly anisotropic cases (AM03:δ = 0.3, AM05:δ = 0.5, AM07:δ = 0.7) showing a smaller increase in temperature.

3.2. Melting and Time Variability

[15] To illustrate the consequences of changes in the thermal structure of the wedge, we postprocess the thermal fields to calculate anhydrous melting at the interior of the wedge, similar to *England and Katz* [2010]. We find which areas of the model domain have exceeded the solidus temperatures, and by how much. This measurement serves as a proxy for the amount of partial melt that is expected from each model: the melt fraction F generated by adiabatic decompression within the above-solidus region scales as $F(T, P) = 0.3(T - T_s(P))$, where P is pressure, T is temperature, and $T_s(P)$ is the solidus temperature [*Elkins-Tanton and Hager*, 2005]. We use the parameterized solidus for anhydrous peridotite of *Till et al.* [2010]:

$$T_s(P) = -3.3313P^2 + 104.05P + 1200 \quad (1)$$

where T_s is in °C and P is given in GPa. We assume a lithostatic pressure with a density $\rho = 3300$ kg/m^3.

[16] Looking at the average excess temperature within the above-solidus region reveals an intriguing result: time variability that is proportional to the strength of the anisotropy. In Figures 4a–4d we plot histograms of model time steps and the corresponding $\langle T - T_s \rangle$ within the melting region. The standard deviation of the results is much wider for the strongly anisotropic case, and decreases with the strength of anisotropy (Figure 4e). It is important to note that the time variability depicted in Figure 4 is not because the anisotropic models take longer to reach steady state. Figure 4f displays time

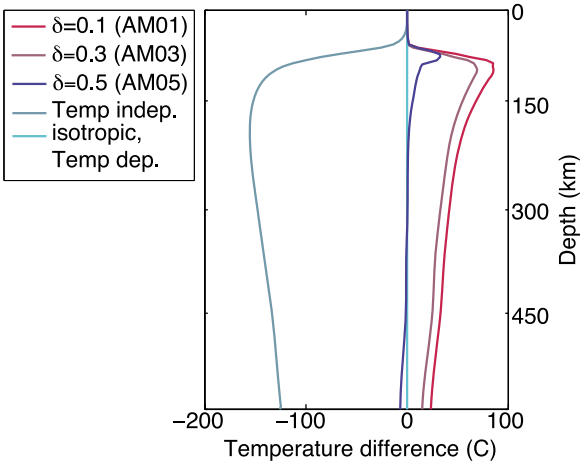

Figure 3. Temperature difference profiles taken at the top of the slab (along a 45° dipping line from the box corner). The curves show the difference in temperature between each model and the reference isotropic, temperature-dependent viscosity model (IM). The anisotropic models show warmer temperatures proportional to the strength of the anisotropy. A model with temperature-independent viscosity (green line) exhibits substantially colder slab top temperatures.

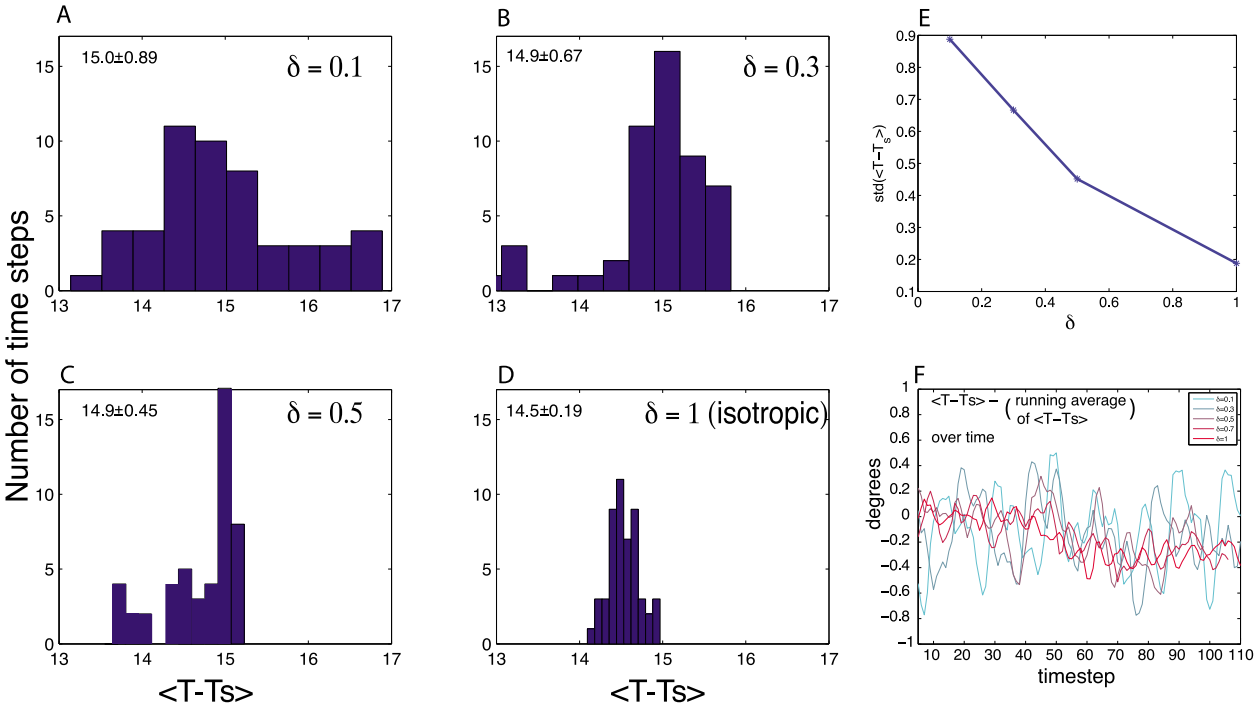

Figure 4. Time variability and the correlation with the strength of anisotropy. (a-d) Histograms showing time variability of the average excess temperature $\langle T - T_s \rangle$ within the melting region. Bar height represents the number of model time steps within each temperature difference interval. The width of the histogram, reflecting the time variability, decreases with the strength of the anisotropy. (e) The correlation between the standard deviation of each distribution and the strength of anisotropy (δ value). (f) Time series of $\langle T - T_s \rangle$ minus a running average of $\langle T - T_s \rangle$ reveals the difference in "noisiness" levels between the different models.

series of $\langle T - T_s \rangle$, and it is clear that the plots for less isotropic models are smoother. Plotting the deviation of the measured quantity $\langle T - T_s \rangle$ from a running average over time (Figure 4f) shows that the anisotropic models retain their "noisiness" over time.

4. Discussion

[17] The warmer temperature along the slab-wedge interface in the anisotropic models may lead to lower viscosities in this area and influence dehydration processes and flux melting. This heating is a result of the flow geometry: the anisotropic viscosity and the strong alignment resist the sharp turn at the wedge tip, and the stream lines are forced to make a wider turn. Thus, the isotherms are pushed against the slab, making the contact region warmer. Temperatures higher by 35° directly along the slab-wedge interface, or close to 100° slightly above it, might be enough to cause melting of water-saturated sediments (based on the solidus by *Nichols et al.* [1994] and P-T diagrams from *Johnson and Plank* [1999]). Such melting is required by geochemical observations at arc volcanoes [*Johnson and Plank*, 1999]. As an example, we plot slab surface temperature profiles for IM and for AM01 on phase stability diagrams calculated by *Hacker* [2008] (MORB in Figure 5; altered oceanic crust and sediments in Figure S2). The difference between IM (black line) and AM01 can lead, for the most part, to shallowing of the depth of dehydration and breakdown of minerals.

[18] It is important to quantify the sensitivity of our model results to the addition of anisotropic viscosity, with the known effect of including temperature-dependent viscosity. In Figure 3 we plot the temperature along the slab-wedge interface for a model with viscosity that does not depend on temperature. We find that in such a model, slab surface temperatures are up to 150° colder compared to the temperature-dependent, isotropic model. This means that the model results, while clearly influenced by the addition of anisotropic viscosity, are 4 to 5 times more sensitive to the dependence of viscosity on temperature.

[19] Another parameter which directly controls the amount of melting, the mantle potential tempera-

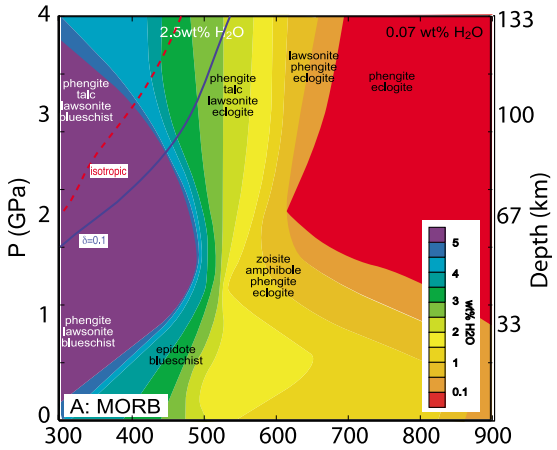

Figure 5. Slab top temperature profiles for isotropic (solid blue) and anisotropic ($\delta = 0.1$, dashed red) plotted on top of a phase stability for MORB taken from *Hacker* [2008].

ture T_p, is also a free parameter in our models. The potential temperature of the mantle is not very well constrained, and estimates range between 1315°C *McKenzie et al.*, 2005] and 1450°C [*Anderson*, 2000]. We compare the sensitivity of our model results to anisotropy with the influence of changing T_p. Figure 6 shows the specific case of melt production rate in the above-solidus region. Adding anisotropy increases the total melt production rate. This increase depends on the assumed value of the mantle potential temperature (T_p). However, the selection of T_p has a larger effect on the total melt production rate. For instance, changing T_p by 20° increases the melt production rate by a factor of between 3 and 4, while changing adding strong anisotropy ($\delta = 0.1$) increases the melt production rate by a factor of about 1.5. The reason is simple: adding anisotropy only changes the shape of the melting region slightly, but changing T_p makes this region significantly larger. We also find that adding anisotropy increases the average excess temperature in the above-solidus region ($\langle T - T_s \rangle$) by about 9%. On the other hand, the average excess temperature appears to be linearly proportional to T_p, so a change of 50° in T_p leads to an increase of 15% in $\langle T - T_s \rangle$.

[20] One important phenomenon introduced by the addition of anisotropic viscosity is time variability. This can not be attributed to other parameters such as potential temperature, temperature-dependent viscosity, or lower effective viscosity. A time variability such as that shown by our anisotropic models may lead to time-dependent volcanism even without changes in slab age, dip or velocity. The main source of time variability in the anisotropic models is the heterogeneity in effective viscosity of the material moving through the wedge, caused by incomplete alignment of the anisotropic material. This heterogeneity leads to a noisier velocity field. An additional, smaller, source of noise might lay in the numerical solution itself, due to grid resolution or particle discretization (see Figure S1). Two points are important to address here. First, we point out again that the time variability depends on a magnitude of anisotropy, as demonstrated in Figure 4. Therefore, if the materials in the mantle wedge are only weakly mechanically anisotropic, anisotropy-induced temporal changes are weaker. Second, we note that the fabric in the models presented here starts with random orientations. In the mantle, material in subduction zones may have a more uniform preexisting fabric, a remnant from prior deformation. Models run with prescribed initial preferred orientations were strongly influenced by the choice of that fabric and displayed strongly transient behavior, in the dry melting region in particular. This region, at the core of the mantle wedge, has relatively low strain rates, especially when anisotropy leads to focusing of the strain in narrow shear zones along the interfaces between the wedge and the slab or the overriding plate. Thus, it takes a very long time for the material in the interior to realign or to move away, and any initially prescribed fabric will alter the thermal, and melting, behavior. In Figure S3 we use color to represent the orientations of each director in the wedge corner. The distribution of colors shows that even after a very long

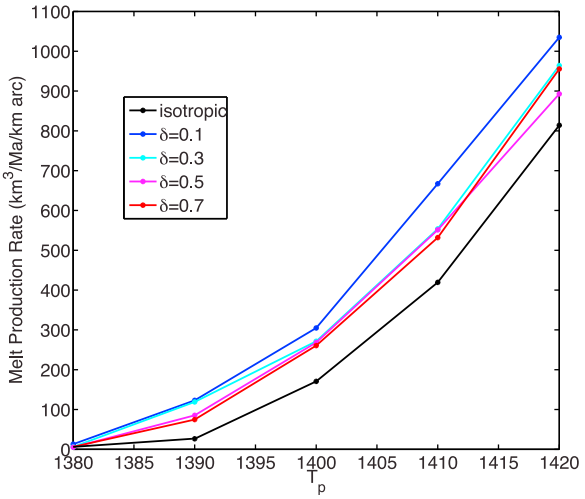

Figure 6. Sensitivity of calculated melt production rates: comparing the influence of anisotropy versus the influence of the chosen value for mantle potential temperature.

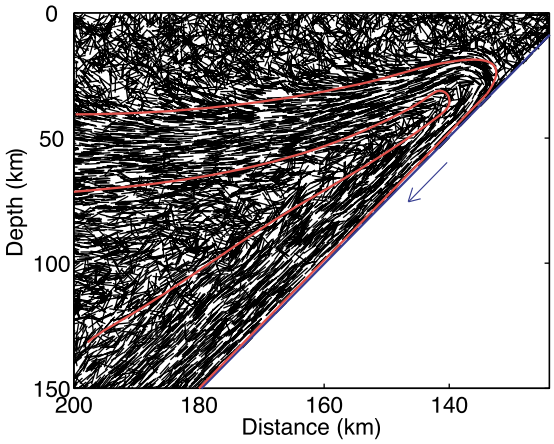

Figure 7. Orientation of easy glide planes (black bars) calculated in AM01. The strong LPO is concentrated in two regions: along the top of the slab and below the base of the overriding lithosphere. At the heart of the mantle wedge, orientation appear random and LPO is weak. The LPO in the overriding plate is weak as well, displaying the initial random orientation that got frozen in. The red lines show streamlines through the models.

time, the material in the wedge is not fully aligned, explaining some of the erratic behavior of this model.

[21] An inherent part of our modeling technique is the tracking of the evolution of preferred orientations in the mantle wedge in great detail. Previous models have either used simplified techniques such as the tracking of finite strain ellipses [*Hall et al.*, 2000; *Long et al.*, 2007], or limited their LPO modeling to a small region within the mantle wedge [*Kneller et al.*, 2008]. The LPO field resulting from our models, partly shown in Figures 7 and S3 is in general agreement with previous approximations [e.g., *Long et al.*, 2007]. It demonstrates that the strongest fabric resides immediately above the slab and below the overriding lithospheric lid, and that the fabric in the center of the wedge is weak. This information is useful for locating the source of anisotropic signals measured at subduction zones by seismic techniques. The concentration of aligned material in the two boundary layers, leaving the center of the wedge poorly aligned, may explain the poor correlation between slab dip and delay times of shear wave splitting [*Long and Silver*, 2008, Figure S4].

[22] Our models assume A type fabric (slip on the (010)[100] system) for the olivine in the wedge. It has been shown that at the presence of water, B type fabric (slip on the (010)[001] system) can develop [e.g., *Jung and Karato*, 2001]. The mantle wedge may be a location for B type fabric, and this fabric is often invoked to explain observations of trench-parallel seismic anisotropy. In natural samples, both A type [*Mehl et al.*, 2003] and B type [*Mizukami et al.*, 2004] fabrics have been observed. An interesting direction of future research is to examine the influence of a changing dominant slip system on the dynamics of flow in the mantle wedge.

5. Summary

[23] We include anisotropic viscosity in kinematic thermal models of subduction zone wedge flow. All our models, with the exception of one control case, have temperature-dependent viscosity, essential for getting dry melting in the wedge. Anisotropic viscosity leads to significant changes in the thermal structure of subduction zone wedges compared to the isotropic model: the temperature at the slab-wedge interface increases by 35 degrees or more, and the melting becomes time dependent. The time variability results from fluctuations in the velocity field caused by the anisotropic viscosity. This time variability is on relatively short time scales and may provide an explanation for observed time variations in melt extent. Therefore, anisotropic viscosity and the effective viscosity heterogeneity play an important role in determining the thermal structure of the mantle wedge and the melt produced in it.

Acknowledgments

[24] We are grateful to Marc Spiegelman for his tremendous help and invaluable advice regarding the work we present here. Comments by two anonymous reviewers, as well as the editor, helped improve the content of this paper. We thank Christy Till, Tim Grove, Lindy Elkins-Tanton, Maureen Long, Peter van Keken, and Mark Behn, whose suggestions helped guide this work. The research presented here was supported by NSF grant EAR-0409564 and the LDEO Postdoctoral Fellowship to EL.

References

Anderson, D. L. (2000), Thermal state of the upper mantle: No role for mantle plumes, *Geophys. Res. Lett.*, *27*, 3623–3626.

Billen, M. I., M. Gurnis, and M. Simons (2003), Multiscale dynamics of the Tonga-Kermadec subduction zone, *Geophys. J. Int.*, *153*, 359–388.

Castelnau, O., D. K. Blackman, R. A. Lebensohn, and P. Ponte (2008), Micromechanical modeling of the viscoplastic behavior of olivine, *J. Geophys. Res.*, *113*, B09202, doi:10.1029/2007JB005444.

Christensen, U. (1987), Some geodynamical effects of anisotropic viscosity, *Geophys. J. R. Astron. Soc.*, *91*, 711–736, doi:10.1111/j.1365-246X.1987.tb01666.x.

Drury, M. R., R. L. M. Vissers, D. van der Wal, and E. H. Hoogerduijn Strating (1991), Shear localisation in upper mantle peridotites, *Pure Appl. Geophys.*, *137*, 439–460, doi:10.1007/BF00879044.

Durham, W. B., and C. Goetze (1977), Plastic flow of oriented single crystals of olivine 1. Mechanical data, *J. Geophys. Res.*, *82*, 5737–5754.

Elkins-Tanton, L. T., and B. H. Hager (2005), Giant meteoroid impacts can cause volcanism, *Earth Planet Sci. Lett.*, *239*, 219–232, doi:10.1016/j.epsl.2005.07.029.

England, P. C., and R. F. Katz (2010), Melting above the anhydrous solidus controls the location of volcanic arcs, *Nature*, *467*, 700–703, doi:10.1038/nature09417.

Gurnis, M. (1993), Phanerozoic marine inundation of continents driven by dynamic topography above subducting slabs, *Nature*, *364*, 589–593.

Hacker, B. R. (2008), H_2O subduction beyond arcs, *Geochem. Geophys. Geosyst.*, *9*, Q03001, doi:10.1029/2007GC001707.

Hall, C. E., K. M. Fischer, E. M. Parmentier, and D. K. Blackman (2000), The influence of plate motions on three-dimensional back arc mantle flow and shear wave splitting, *J. Geophys. Res.*, *105*, 28,009–28,034.

Hearn, E. H., E. D. Humphreys, M. Chai, and M. Brown (1997), Effect of anisotropy on oceanic mantle temperatures, structure and dynamics, *J. Geophys. Res.*, *102*, 11,943–11,956.

Hirth, G. (2002), Laboratory constraints on the rheology of the upper mantle, *Rev. Mineral. Geochem.*, *51*(1), 97–120, doi:10.2138/gsrmg.51.1.97.

Hirth, G., and D. L. Kohlstedt (1995), Experimental constraints on the dynamics of the partially molten upper mantle: Deformation in the diffusion creep regime, *J. Geophys. Res.*, *100*, 1981–2001.

Holtzman, B. K., D. L. Kohlstedt, M. E. Zimmerman, F. Heidelbach, T. Hiraga, and J. Hustoft (2003), Melt segregation and strain partitioning: Implications for seismic anisotropy and mantle flow, *Science*, *301*, 1227–1230.

Honda, S. (1986), Strong anisotropic flow in a finely layered asthenosphere, *Geophys. Res. Lett.*, *13*, 1454–1457.

Johnson, M. C., and T. Plank (1999), Dehydration and melting experiments constrain the fate of subducted sediments, *Geochem. Geophys. Geosyst.*, *1*(12), 1007, doi:10.1029/1999GC000014.

Jung, H., and S. Karato (2001), Water-induced fabric transitions in olivine, *Science*, *293*, 1460–1463.

Karato, S., M. R. Riedel, and D. A. Yuen (2001), Rheological structure and deformation of subducted slabs in the mantle transition zone: implications for mantle circulation and deep earthquakes, *Phys. Earth Planet. Inter.*, *127*, 83–108.

Katagi, T., S. Yoshioka, and M. Hashimoto (2008), Influence of temperature- and depth-dependent viscosity structures on postseismic deformation predictions for the large 1946 Nankai subduction zone earthquake, *Tectonophysics*, *454*, 1–4.

Kelemen, P. B., J. L. Rilling, E. M. Parmentier, L. Mehl, and B. R. Hacker (2003), Thermal structure due to solid-state flow in the mantle wedge beneath arcs, in *Inside the Subduction Factory*, *Geophys. Monogr. Ser.*, vol. 138, edited by J. Eiler, pp. 293–311, AGU, Washington D. C.

Kemp, D. V. (1992), A model for the subduction mechanics of flexible lithosphere and its viscous coupling to the mantle using power-law rheologies, Ph.D. thesis, California Univ., Los Angeles.

Kneller, E. A., M. D. Long, and P. E. van Keken (2008), Olivine fabric transitions and shear wave anisotropy in the Ryukyu subduction system, *Earth Planet. Sci. Lett.*, *268*, 268–282, doi:10.1016/j.epsl.2008.01.004.

Lev, E., and B. H. Hager (2008a), Rayleigh-Taylor instabilities with anisotropic lithospheric viscosity, *Geophys. J. Int.*, *173*, 806–814, doi:10.1111/j.1365-246X.2008.03731.x.

Lev, E., and B. H. Hager (2008b), Prediction of anisotropy from flow models: A comparison of three methods, *Geochem. Geophys. Geosyst.*, *9*, Q07014, doi:10.1029/2008GC002032.

Long, M. D., B. H. Hager, M. V. de Hoop, and R. D. van der Hilst (2007), Two-dimensional modelling of subduction zone anisotropy with application to southwestern Japan, *Geophys. J. Int.*, *170*, 839–856, doi:10.1111/j.1365-246X.2007.03464.x.

Long, M. D., and P. G. Silver (2008), The subduction zone flow field from seismic anisotropy: A global view, *Science*, *319*, 315–318.

McKenzie, D., J. Jackson, and K. Priestley (2005), Thermal structure of oceanic and continental lithosphere, *Earth Planet. Sci. Lett.*, *233*(3–4), 337–349, doi:10.1016/j.epsl.2005.02.005.

Mehl, L., B. R. Hacker, G. Hirth, and P. B. Kelemen (2003), Arc-parallel flow within the mantle wedge: Evidence from the accreted Talkeetna arc, south central Alaska, *J. Geophys. Res.*, *108*(B8), 2375, doi:10.1029/2002JB002233.

Mizukami, T., S. R. Wallis, and J. Yamamoto (2004), Natural examples of olivine lattice preferred orientation patterns with a flow-normal a-axis maximum, *Nature*, *427*, 432–436.

Molnar, P., and T. Atwater (1978), Interarc spreading and Cordilleran tectonics as alternates related to the age of subducted oceanic lithosphere, *Earth Planet. Sci. Lett.*, *41*, 330–340, doi:10.1016/0012-821X(78)90187-5.

Moresi, L., S. Quenette, V. Lemiale, C. Mériaux, B. Appelbe, and H.-B. Mühlhaus (2007), Computational approaches to studying non-linear dynamics of the crust and mantle, *Phys. Earth. Planet. Inter.*, *163*, 69–82, doi:10.1016/j.pepi.2007.06.009.

Mühlhaus, H.-B., L. Moresi, B. Hobbs, and F. Dufour (2002), Large amplitude folding in finely layered viscoelastic rock structures, *Pure Appl. Geophys.*, *159*, 2311–2333.

Nichols, G. T., P. J. Wyllie, and C. R. Stern (1994), Subduction zone melting of pelagic sediments constrained by melting experiments, *Nature*, *371*, 785–788, doi:10.1038/371785a0.

Richter, F. M., and S. F. Daly (1978), Convection models having a multiplicity of large horizontal scales, *J. Geophys. Res.*, *83*, 4951–4956.

Saito, M., and Y. Abe (1984), Consequences of anisotropic viscosity in the Earth's mantle [in Japanese, with English abstract], *J. Seismol. Soc. Jpn.*, *37*, 237–245.

Savage, M. K. (1999), Seismic anisotropy and mantle deformation: What have we learned from shear wave splitting?, *Rev. Geophys.*, *37*, 65–106.

Stein, C., J. Schmalzl, and U. Hansen (2004), The effect of rheological parameters on plate behaviour in a self-consistent model of mantle convection, *Phys. Earth Planet. Inter.*, *142*, 225–255.

Till, C. B., L. T. Elkins-Tanton, and K. M. Fischer (2010), A mechanism for low-extent melts at the lithosphere-asthenosphere boundary, *Geochem. Geophys. Geosyst.*, *11*, Q10015, doi:10.1029/2010GC003234.

Torii, Y., and S. Yoshioka (2007), Physical conditions producing slab stagnation: Constraints of the Clapeyron slope,

mantle viscosity, trench retreat, and dip angles, *Tectonophysics*, *445*, 200–209, doi:10.1016/j.tecto.2007.08.003.

Treagus, S. H. (2003), Viscous anisotropy of two-phase composites, and applications to rocks and structures, *Tectonophysics*, *372*, 121–133.

van Keken, P., B. Kiefer, and S. Peacock (2002), High-resolution models of subduction zones: Implications for mineral dehydration reactions and the transport of water into the deep mantle, *Geochem. Geophys. Geosyst.*, *3*(10), 1056, doi:10.1029/2001GC000256.

van Keken, P. E., C. Currie, S. D. King, M. D. Behn, A. Cagnioncle, J. He, R. F. Katz, S. Lin, E. M. Parmentier, M. Spiegelman, and K. Wang (2008), A community benchmark for subduction zone modeling, *Phys. Earth Planet. Inter.*, *171*(1–4), 187–197, doi:10.1016/j.pepi.2008.04.015.

Wada, I., and K. Wang (2009), Common depth of slab-mantle decoupling: Reconciling diversity and uniformity of subduction zones, *Geochem. Geophys. Geosyst.*, *10*, Q10009, doi:10.1029/2009GC002570.

Wahr, J., and D. Han (1997), Predictions of crustal deformation caused by changing polar ice on a viscoelastic Earth, *Surv. Geophys.*, *18*, 303–312, doi:10.1023/A:1006548312835.